Supporting Information

Tomatis *et al.* 10.1073/pnas.0807989106

SI Materials and Methods

DNA Techniques. DNA preparation and related techniques were performed according to standard protocols (1). Plasmid DNA was isolated by using the Wizard Plus SV Minipreps kit (Promega). DNA was extracted from agarose gels by using QIAEX II kit (Qiagen) or GFX columns (Amersham Pharmacia).

Site-Directed Mutagenesis. Site-directed mutagenesis was performed by using the *megaprimer* PCR method (2). A mutagenic primer was used in conjunction with a suitable forward or reverse primer to obtain a PCR product, which was then used as a megaprimer in a second-stage PCR. For the N70S mutation a DNA fragment containing the N-terminal region of *bcII* gene was amplified by using the ks-reverse primer (TCACACAggAAACAgCTATgAC) and the mutagenic primer N70S (gAAgCAgTTCCCTCgAgCggTCTAgTTC) that introduced the desired mutation and a translationally silent mutation that generates a XhoI restriction site. For the G262S mutation, a DNA fragment containing the C-terminal region of *bcII* gene was amplified by using the ks-forward primer (CgCCAgggTTTTCCCAgTCACgAC) and the mutagenic primer G262S (gCAgTAgTgCCTAgCCATggggAAgTAg) that introduced the desired mutation and a translationally silent mutation that generates a NcoI restriction site. For the first PCR, a total volume of 100 μl containing 50 pmol each of the mutagenic primer and the forward or reverse primer, 0.2 mM each dNTP, 100 ng of template DNA, 2 units of *Vent* DNA polymerase, and 1× *Vent* DNA polymerase buffer was used to amplify a DNA fragment stretching from the region being mutated. PCR reactions were performed on a GeneAmp PCR System 2400 thermocycler (PerkinElmer Life Sciences). Thermocycling was performed with a PCR program of 94 °C 3′/30 × (94 °C 2′, 50 °C 3′, 72 °C 3′) and a final extension step (72 °C for 10 min). The PCR mixture was resolved in a 2% agarose gel containing ethidium bromide, and the *megaprimer* was recovered and purified by using the QIAEX II kit. The second PCR was carried out by using the same DNA template, the megaprimer that codes for the desired mutation and the ks-forward primer. All of the megaprimer recovered from the first PCR was used in the second round of amplification, in a total volume of 100 μl containing 50 pmol of the forward primer, 200 ng of DNA template, 0.2 mM each dNTP, 2 units of *Vent* DNA polymerase, and 1× *Vent* DNA polymerase. The same PCR program was used as mentioned for the first reaction with an annealing temperature of 55 °C. For the N70S mutation, the final amplification product was digested with PstI and BamHI, a fragment of 334 bp (the coding DNA for the N-terminal region of BcII) was purified from a 1% agarose gel, and ligated into the pBCKSCT plasmid digested with the same enzymes to obtain the pBCN70S plasmid. For the G262S mutation, the final product was digested sequentially with PstI and HindIII, a fragment of 365 bp (the coding DNA for the C-terminal region of BcII) was purified from a 1% agarose gel, and ligated back into the pBCKSNT plasmid digested with the same enzymes to obtain the pBCG262S plasmid. To construct the double mutant N70S/G262S BcII, the plasmid pBCN70S was digested sequentially with PstI and BamHI, and a fragment of 334 bp (the coding DNA for the N-terminal region of N70S) was purified from a 1% agarose gel. The plasmid pBCG262S was digested sequentially with PstI and HindIII, and a fragment of 365 bp (the coding DNA for the C-terminal region of G262S BcII) was purified from a 1% agarose gel. These two fragments were used in a double-ligation experiment with the pBluescript II vector digested with BamHI and HindIII to obtain the pBCN70S/G262S plasmid. The mutations N70S and G262S were first corroborated by digestion of the DNA with the restriction endonucleases XhoI and NcoI, respectively. Afterward, the sequences were confirmed by nucleotide sequence analysis with an ABI 3730 Capillary Sequencer via the Sequencing Facility of University of Maine (Orono, ME).

Protein Expression and Purification. Plasmids pBCN70S, pBCG262S, and pBCN70S /G262S were digested with the restriction endonucleases BamHI and HindIII, and the resulting 696-bp fragments were cloned into a pET-Term plasmid digested with the same restriction endonucleases, giving rise to plasmids pET-Term-N70S, pET-Term-G262S, and pET-Term-N70S/G262S, respectively. The expression vector pET-Term is a derivative of the pETGEX vector that allows overexpression of the protein of interest as an amino-terminal fusion protein to the enzyme GST from *Schistosoma japonicum*, under control of the T7 promoter (3). All of the mutants' proteins were overexpressed in *Escherichia coli* BL21(DE3) *pLysS′* as fusion proteins with GST, purified and quantified as described in ref. 4. The metal content was determined in protein samples dialyzed 4 times against metal-free 10 mM Hepes, pH 7.5, 0.2 M NaCl, at 4 °C, by using the colorimetric reagent 4-(2-pyridylazo)-resorcinol (PAR) under denaturing conditions (5).

X-ray Crystallography. The data were processed by using Denzo (6) and the CCP4 (7) programs Scala (8) and Truncate (9). Initial phases were obtained from Molecular Replacement using Phaser (10). The structure was refined by using CNS v1.1 (11) and Phenix v 1.3 (12), and the model was build by using Quanta (Accelrys) and Coot (13). Data collection and refinement statistics are detailed in supporting information (SI) Table S1.

Electronic Spectroscopy of Co(II) Derivatives. The apoproteins were obtained as described elsewhere (3, 14). Titration of metal-free enzyme mutants N70S BcII, G262S BcII, and N70S/G262S BcII with Co(II) was followed by absorption spectroscopy. Electronic absorption spectra were recorded in a Jasco V-550 spectrophotometer thermostated with a water circulator at 30 °C, and difference spectra were obtained by subtracting the spectrum of the corresponding apoprotein. Different preparation of apoproteins (≈200 μM) in 10 mM Hepes, pH 7.5, 0.2 M NaCl were titrated with a 5 mM $CoSO_4$ stock solution prepared in the same buffer.

Single Turnover Kinetic Studies. Changes in the visible spectra of nitrocefin during hydrolysis with WT BcII and G262S BcII enzymes were followed with a stopped-flow system associated to a photodiode-array detector. Experiments were carried out on a SX.18-MVR stopped-flow spectrometer (Applied Photophysis) as reported. The measurements were performed in 100 mM Hepes, pH 7.5, 0.2M NaCl, 1 mM Zn(II), and the whole sample was kept at 6 °C. Data from different experiments were corrected for the instrument dead time (2 ms). A set of scans were made in the wavelength range of 300 to 730 nm with a integration time of 1.25 ms for a total acquisition time of 0.025 s during a single-turnover experiment using 200 μM enzyme and 60 μM nitrocefin. Absorbance changes, the consumption of nitrocefin at 390 nm, formation of the product at 490 nm, and the absorbance at 665 nm, that occurred during the single-turnover reaction hydrolysis of 12.85 μM nitrocefin by 47 μM G262S BcII

at 6 °C were also monitored with an absorbance photomultiplier. The molar extinction coefficients of nitrocefin used are: substrate $\varepsilon_{390\ nm}$ = 18,000 M^{-1} cm^{-1}; product $\varepsilon_{390\ nm}$ = 5,800 M^{-1} cm^{-1}, $\varepsilon_{490\ nm}$ = 17,500 M^{-1} cm^{-1}. The absorbance spectrum of the intermediate has a intense absorbance band at 665 nm with a molar coefficient of 34,000 M^{-1} cm^{-1}. Steady-state kinetic parameters in the same conditions used for the single-turnover experiments were carried out with 2 nM enzyme and 20 μM nitrocefin by recording the whole reaction time curse of nitrocefin product formation at 490 nm, and fitting to the integrated form of the Michaelis–Menten equation.

Molecular Dynamics simulations. The structure of di-Zn(II) BcII from *Bacillus cereus* [PDB ID code 1BC2 (15)] was selected as the reference starting structure for all our calculations. Loop L3, which is not present in the corresponding coordinates file, was reconstructed and modeled as reported in ref. 16. The starting structures for G262S BcII and N70S/G262S BcII were obtained by superimposing the backbone atoms of the serine residues over those of the corresponding wild-type residues. The resulting $\chi 1$ and $\chi 2$ angles were verified to fall in the most favorable regions. Each system was immersed in a box (85.6 Å × 80.3 Å × 85.9 Å) of water molecules (≈17,000), with 4 chloride anions for neutralizing the excess charge. The force-field parameters for the protein frame, the counterions, and water are those of the AMBER PARM98 (17) and TIP3P (18), respectively. For the coordination sphere of the Zn(II) ions, we followed the same scheme as in ref. 16. For the antibiotics, the gaff force field was used (19), as for the charges. Electrostatic interactions were computed by using the Particle Mesh Ewald (PME) algorithm (20). A cutoff of 12 Å was used for van der Waals and for short-range component of electrostatic interactions. Bonds involving hydrogen atoms were constrained by using the SHAKE algorithm (21). An integration time step of 1.5 fs was used. Loop L3 and the side chains of mutations were first-energy-minimized by using a steepest descent algorithm. The systems were initially relaxed with 5,000 steps of optimization of the solvent, whereas the protein was held fixed, followed by 5,000 steps of optimization of the whole system. The systems were slowly heated to 300 K performing runs at constant volume and constant temperature by using Langevin Dynamics (22, 23). Constant temperature and pressure (1 atm, 300 K) molecular dynamics (MD) runs were finally performed (24). The pressure coupling was accomplished with Langevin piston (25) and the temperature with the Nose'-Hoover method (26, 27). Ten nanoseconds of trajectory were produced for every system, with the aim of NAMD programs (22, 23). Subsequently, Cefalexin was docked inside the last MD snapshots of the 3 structures. The 3 Michaelis complexes underwent the same computational protocol as the free states.

In Vitro Stability. Samples at different Gdn-HCl concentrations were prepared individually and left to equilibrate for 2 h. The concentration of Gdn-HCl was determined by using the refractive index and the protein concentration was 3 μM. Emission was measured at 368 nm with excitation at 280 nm and a 5 nm bandwidth. Equilibrium denaturation transitions followed by fluorescence were analyzed by using a 2-state (Eq. **1**) model, which includes parameters for a linear pre- and posttransition dependence on denaturant concentration; or a 3-state model (Eq. **2**), including an intermediate species (I).

$$F_{obs}=((F_n+S_{ln}[\text{Gdn-HCl}])+F_u+S_{lu}[\text{Gdn-HCl}]K_u)/(1+K_u) \quad [1]$$

$$F_{obs}=f_n(F_n+S_{ln}[\text{Gdn-HCl}])+f_i(F_i+S_{li}[\text{Gdn-HCl}]) +f_u(F_u+S_{lu}[\text{Gdn-HCl}]) \quad [2]$$

where

$K_u = e(-\Delta G_{nu} - m_{nu}\,[\text{Gdn-HCl}])/RT$
$f_n = 1/(1 + K_{ni} + K_{ni}\,K_{iu})$
$f_i = K_{ni}/(1 + K_{ni} + K_{ni}\,K_{iu})$
$f_u = (K_{ni}\,K_{iu})\,/(1 + K_{ni} + K_{ni}\,K_{iu})$
$K_{ni} = e(-\Delta G_{ni} - m_{ni}\,[\text{Gdn-HCl}])/RT$
$K_{iu} = e(-\Delta G_{iu} - m_{iu}\,[\text{Gdn-HCl}])/RT$
$C_m = \Delta G_{nu}/m_{nu}$
$C_{m1} = \Delta G_{ni}/m_{ni}$
$C_{m2} = \Delta G_{iu}/m_{iu}$

F_{obs} is the intensity of emitted fluorescence for each protein, [Gdn-HCl] is the concentration of guanidine hydrochloride, F_n is the intensity of emitted fluorescence of the native protein, S_{ln} is the slope of the pretransition baseline due to the effect of Gdn-HCl on the fluorescence of the native protein, F_u is the fluorescence of the unfolded protein, S_{lu} is the slope of the pretransition baseline due to the effect of Gdn-HCl on the fluorescence of the unfolded protein, ΔG_{nu} is the free-energy change from protein unfolding, m_{nu} is the slope of a plot of observed ΔG_{nu} ($-RT$ ln U/N) against [Gdn-HCl], R is the gas constant, and T is the absolute temperature. The error limits shown are the standard deviations of the parameter estimates as determined by nonlinear least-squares fitting. In the 3-state model, according to Eq. **2**, the symbols have essentially the same definition as given for Eq. **1**, except for the inclusion of an intermediate species (I). ΔG_{ni} corresponds to the free energy of the N to I transition extrapolated to zero denaturant, and ΔG_{iu} corresponds to the free energy of the I to U transition. The thermodynamic parameters describing the equilibrium folding process of the 5 proteins were obtained from fitting of the experimental equilibrium unfolding curves by using the Solver routine from Excel.

Protein Extracts Isolation and Western Blot Analysis. Overnight cultures of *E. coli* JM109 carrying MβL plasmids (plasmid pKPs) were grown at 37 °C in 10 ml of LB medium in the presence of kanamycin (50 μg/ml). MβL expression was induced by adding 500 μM IPTG to the culture. When the cells reached a log phase of growth (OD_{600} 0.6), they were harvested by centrifugation at 5,000 × g for 10 min. The supernatant containing extracellular medium was set aside. The soluble periplasmic fraction was released by osmotic shock by resuspending the pellet in 5 ml of 30 mM Tris, 1 mM PMSF, 20% sucrose buffer (pH 8.0) for 10 min at room temperature, centrifuging at 5000 × g for 10 min, and resuspending the pellet in 2 ml of cold $MgSO_4$ for 10 min at 10 °C. After centrifugation at 5000 × g for 10 min, the supernatant contained the soluble periplasmic proteins. Proteins were separated by SDS/PAGE by using 14% gels with an acrylamide:bisacrylamide ratio of 29:1 in the Laemmli buffer system. The amounts seeded in each lane were standardized according to $OD_{600\ nm}$ of the cellular cultures. Proteins were transferred to a nitrocellulose membrane. Membranes were stained with 0.1% Ponceau S to confirm equal protein transfer, incubated with a rabbit anti-BcII lactamase antibody followed by alkaline phosphatase-labeled anti-rabbit IgG second antibody, and revealed by using 5-bromo-4-chloro-3-indolyl phosphate and nitroblue tetrazolium chromogenic substrate reaction.

1. Sambrook J, Fitsch EF, Maniatis T (1989) *Molecular Cloning. A Laboratory Manual* (Cold Spring Harbor Lab Press, Cold Spring Harbor, NY).
2. Barik, S (1996) *In Vitro Mutagenesis Protocols*, ed Trower MK (Humana Press, Totowa, NJ), pp 203–215.
3. Orellano EG, Girardini JE, Cricco JA, Ceccarelli EA, Vila AJ (1998) Spectroscopic characterization of a binuclear metal site in Bacillus cereus beta-lactamase II. *Biochemistry* 37:10173–10180.
4. Paul-Soto R, *et al.* (1999) Mono- and binuclear Zn2+-beta-lactamase. Role of the conserved cysteine in the catalytic mechanism. *J Biol Chem* 274:13242–13249.

5. Hunt JB, Neece SH, Ginsburg A (1985) The use of 4-(2-pyridylazo)resorcinol in studies of zinc release from Escherichia coli aspartate transcarbamoylase. *Anal Biochem* 146:150–157.
6. Otwinowski Z, Minor W (1997) Processing of X-ray diffraction data collected in oscillation mode. *Methods Enzymol* 276:307–325.
7. Collaborative Computational Project Number 4 (1994) The *CCP*4 suite: Programs for protein crystallography. *Acta Crystallogr D Biol Crystallogr* 50:760–763.
8. Evans PR (1993) Data reduction. Data collection & processing. *Proceedings of CCP4 Study Weekend* (SERC Daresbury Laboratory, Warrington, UK), pp 114–122.
9. French S, Wilson K (1978) Treatment of negative intensity observations. *Acta Crystallogr A* 34:517–525.
10. McCoy AJ, *et al.* (2007) Phaser crystallographic software. *J Appl Crystallogr* 40:658–674.
11. Brunger AT, *et al.* (1998) Crystallography & NMR system: A new software suite for macromolecular structure determination. *Acta Crystallogr D Biol Crystallogr* 54:905–921.
12. Adams PD, *et al.* (2002) PHENIX: building new software for automated crystallographic structure determination. *Acta Crystallogr D Biol Crystallogr* 58:1948–1954.
13. Emsley P, Cowtan K (2004) Coot: Model-building tools for molecular graphics. *Acta Crystallogr D Biol Crystallogr* 60:2126–2132.
14. Llarrull LI, Tioni MF, Kowalski J, Bennett B, Vila AJ (2007) Evidence for a dinuclear active site in the metallo-beta-lactamase BcII with substoichiometric Co(II). A new model for metal uptake. *J Biol Chem* 282:30586–30595.
15. Fabiane SM, *et al.* (1998) Crystal structure of the zinc-dependent beta lactamase from Bacillus cereus at 1.9 A resolution: Binuclear active site with features of a mononuclear enzime. *Biochemistry* 37:12404–12411.
16. Dal Peraro M, Vila AJ, Carloni P (2004) Substrate binding to mononuclear metallo-beta-lactamase from Bacillus cereus. *Proteins* 54:412–423.
17. Case DA, *et al.* (2002) *AMBER 7* (University of California, San Francisco).
18. Jorgensen WL, Chandrasekhar J, Madura J, Impey RW, Klein ML (1983) Comparison of simple potential functions for simulating liquid water. *J Chem Phys* 79:926–935.
19. Wang JM, Wolf RM, Caldwell JW, Kollman PA, Case DA (2004) Development and testing of a general amber force field. *J Comput Chem* 25:1157–1174.
20. Darden T, York D, Pedersen L (1993) Particle Mesh Ewald: An N.Log(N) method for Ewald sums in large systems. *J Chem Phys* 98:10089–10092.
21. Ryckaert JP, Ciccotti G, Berendsen HJC (1977) Numerical-Integration of cartesian equations of motion of a system with constraints: Molecular-dynamics of N-alkanes. *J Comput Phys* 23:327–341.
22. Nelson MT, *et al.* (1996) NAMD: A parallel, object oriented molecular dynamics program. *Int J Supercomput Appl High Perform Comput* 10:251–268.
23. Phillips JC, *et al.* (2005) Scalable molecular dynamics with NAMD. *J Comput Chem* 26:1781–1802.
24. Martyna GJ, Tobias DJ, Klein ML (1994) Constant-Pressure molecular-dynamics algorithms. *J Chem Phys* 101:4177–4189.
25. Feller SE, Zhang YH, Pastor RW, Brooks BR (1995) Constant-pressure molecular-dynamics simulation: the Langevin piston method. *J Chem Phys* 103:4613–4621.
26. Hoover WG (1985) Canonical dynamics: Equilibrium phase-space distributions. *Phys Rev A* 31:1695–1697.
27. Nose S (1984) A molecular-dynamics method for simulations in the canonical ensemble. *Mol Phys* 52:255–268.
28. Rasia RM, Vila AJ (2003) Mechanistic study of the hydrolysis of nitrocefin mediated by B. cereus metallo-β-lactamase. *Arkivoc*, X, 507–516.

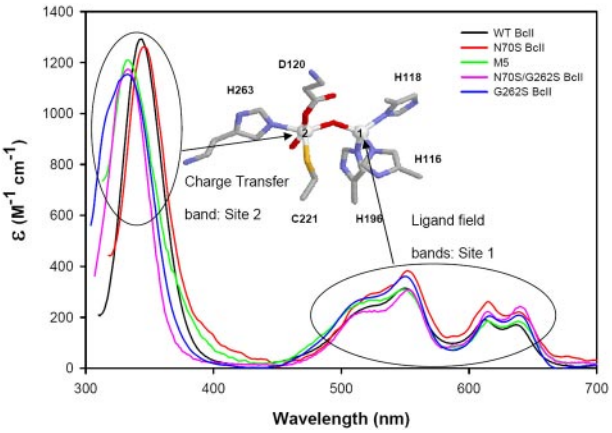

Fig. S1. Electronic spectra of Co(II)-substituted WT BclI, M5, G262S BclI, N70S BclI, and N70S/G262S BclI in 10 mM Hepes (pH 7.5), 0.2 M NaCl.

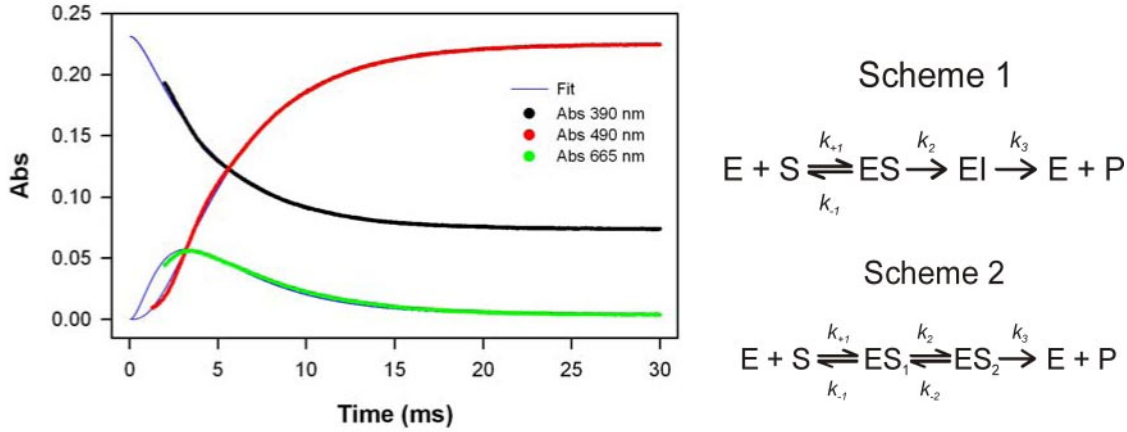

Fig. S2. Single-turnover hydrolysis of 12.85 μM nitrocefin by 47 μM G262S BcII at 6 °C, measured by using an absorption photomultiplier detector in a stopped-flow system. The consumption of nitrocefin (S) at 390 nm is shown in black, formation of the product (P) at 490 nm in red, and the absorbance (EI) at 665 nm in green. The experimental progress curves were fitted using the numerical integration algorithm implemented on the software *Dynafit* (blue lines). The best minimal model that accounts for the experimental data is shown in Scheme 1. This model involves three steps: substrate binding, formation of the intermediate, and product release. The individual kinetic constants obtained by using *Dynafit* were: k_{+1} (s^{-1} μM^{-1}) = 14.7 ± 0.146; k_{-1} (s^{-1}) = 229 ± 5.06; k_{+2} (s^{-1}) = 363 ± 1.64; and k_{+3} (s^{-1}) = 994 ± 2.71. Steady-state kinetic constants [k_{cat} (s^{-1}) = 265, K_M (μM) = 42.6] and the calculated values [k_{cat} (s^{-1}) = 231; K_M (μM) = 43.2] were very similar. The simulated individual kinetics values were obtained by using the following equations:

$$k_{\text{cat}} = (k_{+2}k_{+3})/(k_{+2} + k_{+3})$$

$$K_{\text{M}} = (k_{-1}k_{+3})/(k_{+1}k_{+2}).$$

The minimal model that describes nitrocefin hydrolysis by WT BcII as reported by Rasia *et al.* (28) is shown in Scheme 2. The kinetic constants for this model are: k_{+1} (s^{-1} μM^{-1}) = 100 (fixed); k_{-1} (s^{-1}) = 11,000 ± 280; k_{+2} (s^{-1}) = 4,400 ± 90; k_{-2} (s^{-1}) = 55.6 ± 0.3; and k_{+3} (s^{-1}) = 4.7 ± 0.01.

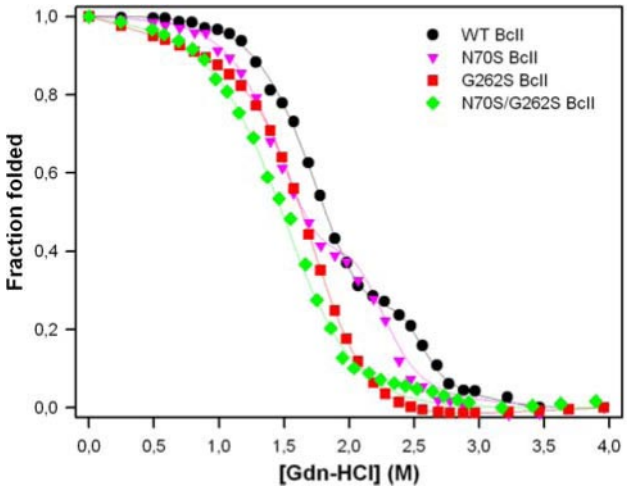

Fig. S3. Equilibrium denaturation curves of WT BclI, G262S BclI, N70S BclI, and N70S/G262S BclI in 50 mM Hepes (pH 7.5), 0.2 M NaCl at different guanidinium hydrochloride concentrations monitored by fluorescence spectroscopy. The lines correspond to a fit of the experimental to a 3-state (WT BclI and N70S BclI) or a 2-state model (G262S BclI and N70S/G262S BclI). The calculated ΔG_u (kcal/mol) values are: 18.5 (WT BclI), 12.9 (N70S BclI), 4.56 (G262S BclI), and 3.28 (N70S/G262S BclI).

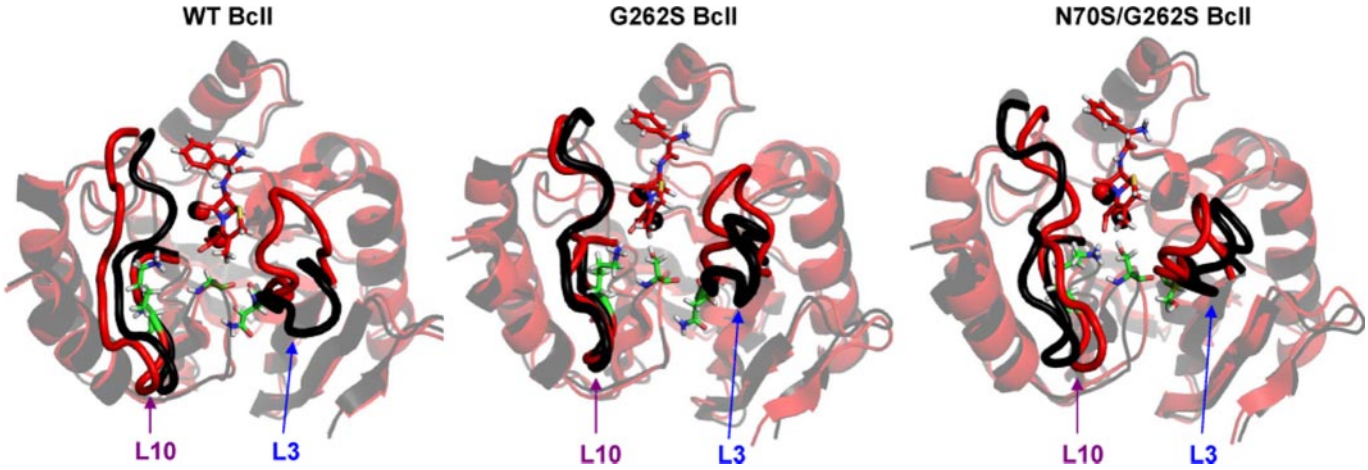

Fig. S4. Superposition of the structures after a 10-ns molecular dynamics calculation of the free (black) and cephalexin-bound (red) WT BcII, G262S BcII, and N70S/G262S BcII. The substrate cephalexin, residues 70, 262, and 224 are shown in sticks and Zn(II) ions are shown as spheres. The 2 loops flanking the active site (L3 and L10) are highlighted.

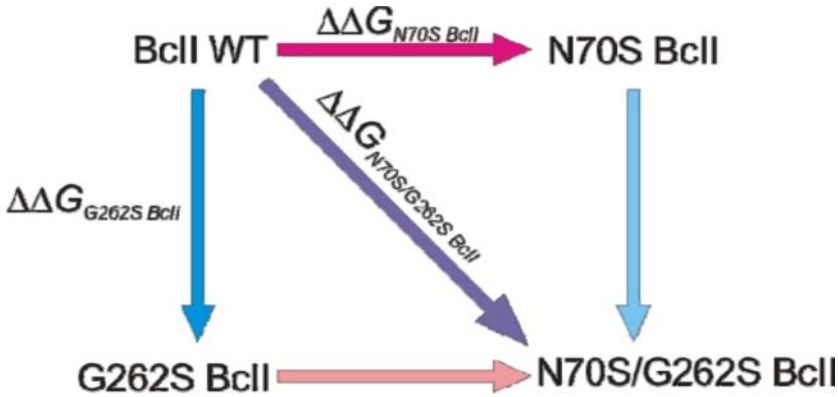

Fig. S5. Double mutant cycle.

Table S1. X-ray refinement statistics

Resolution, Å	2.8
R_{work}/R_{free}	19.02 / 26.35
Number of atoms	3,430
Protein	3,384
Ligand/ion	4
Water	42
B-factors	
Protein	61.5
Ligand/ion	53.5
Water	35.62
rms deviations	
Bond lengths, Å	0.006
Bond angles, °	0.887

Table S2. Kinetic parameters for the hydrolysis of different β-lactam substrates

	G262S BcII			N70S BcII			N70S/G262S BcII			M5			WT BcII		
	k_{cat}	K_M	k_{cat}/K_M	k_{cat}	K_M	k_{cat}/K_M	k_{cat}	K_M	k_{cat}/K_M	k_{cat}	K_M	k_{cat}/K_M	k_{cat}	K_M	k_{cat}/K_M
PEN	320	150	2.13×10^6	543	>3.200	1.69×10^5	636	172	3.69×10^6	570	574	9.93×10^5	1,020	662	1.54×10^6
IMI	40.1	227	1.76×10^5	ND	>3.000	$\approx 1 \times 10^5$	93.2	63.1	1.47×10^6	129	721	1.79×10^5	279	687	4.06×10^5
NTR	680	50.2	1.36×10^7	17.3	14.5	1.19×10^6	460	30.2	1.52×10^7	81.3	27.8	2.92×10^6	30.1	9.82	3.07×10^6
CTX	87.3	60.2	1.45×10^6	115	113	1.01×10^6	182	32.6	5.58×10^6	44.9	30.3	1.49×10^6	80.5	43.3	1.86×10^6
CLX	70.4	217	3.24×10^5	2.05	331	6.19×10^3	221	146	1.51×10^6	41.2	209	1.97×10^5	3.32	125	2.65×10^4

Units: k_{cat} (s^{-1}), K_M (μM), and k_{cat}/K_M (s^{-1} M^{-1}). Conditions: 10 mM Hepes, 0.2 M NaCl, 50 μg/ml BSA, and 20 μM Zn(II) at pH 7.5 and 30 °C. The reported values are the average of at least 3 independent determinations. Standard deviation values were <5%. ND, not determined

Table S3. Thermodynamic parameters for the double mutants cycle

	$\Delta\Delta G_{G262S\ BclI}$	$\Delta\Delta G_{N70S\ BclI}$	$\Delta\Delta G_{N70S/G262S\ BclI}$	ΔG_I
PEN	−0.194	1.32	−0.524	−1.65
IMI	0.501	0.840	−0.771	−2.11
NTR	−0.893	0.568	−0.959	−0.635
CTX	0.149	0.366	−0.659	−1.17
CLX	−1.50	0.872	−2.42	−1.79

$\Delta\Delta G_x = -RT \ln (K_x/K_{WT})$, $\Delta G_I = \Delta\Delta G_{xy} - (\Delta\Delta G_x + \Delta\Delta G_y)$
Units: $\Delta\Delta G$ and ΔG kcal ($mol^{-1}\ K^{-1}$)